A Closed Cavity Ultrasonic Resonator Formed by Graphene/PMMA Membrane for Acoustic Application

Citation for published version:
Xu, J, Wood, G, Mastropaolo, E, Lomax, P, Newton, MJ & Cheung, R 2023, 'A Closed Cavity Ultrasonic Resonator Formed by Graphene/PMMA Membrane for Acoustic Application', *Micromachines*, vol. 14, no. 4, 810. https://doi.org/10.3390/mi14040810

Digital Object Identifier (DOI):
10.3390/mi14040810

Link:
Link to publication record in Edinburgh Research Explorer

Document Version:
Peer reviewed version

Published In:
Micromachines

Article

The Closed Cavity Ultrasonic Resonator Formed by Graphene/PMMA Membrane for Acoustic Application

Jing Xu [1,3,*], Graham S. Wood[1], Enrico Mastropaolo [1,†], Petter Lomax [1] , Michael Newton [2] and Rebecca Cheung [1,*]

1 the School of Engineering, Institute for Integrated Micro and Nano Sys-tems, University of Edinburgh, Edinburgh, EH9 3FF, U.K.
2 the Acoustics and Audio Group, University of Edinburgh, Edinburgh, EH8 9DF, U.K.
3 AAC Technologies (Scotland) Limited, Edinburgh, EH3 8EG, U.K.

* Correspondence: xujing6@aactechnologies.com, r.cheung@ed.ac.uk;

† Deceased 15th July 2019

Abstract: A graphene/poly (methyl methacrylate) (PMMA) closed cavity resonator with the resonant frequency at around 160 kHz has been fabricated. The 6-layer graphene with 450 nm PMMA laminated layer has been dry transferred onto the closed cavity with the air gap of 105 μm. The resonator has been actuated in atmosphere and room temperature by mechanical, electrostatic and electro-thermal methods. The (1,1) mode has been observed to dominate the resonance, which suggests the graphene/PMMA membrane has been perfectly clamped and seals the closed cavity. The degree of linearity of the membrane's displacement versus the actuation signal has been determined. The resonant frequency has been observed to be tuned to about 4% by applying AC voltage through the membrane. The strain has been estimated to be around 0.08%. This research puts forward a graphene-based sensor design for acoustic sensing.

Keywords: graphene, ultrasound, MEMS, resonator

1. Introduction

Graphene has raised many attractions from the research and industrial community since it was discovered [1] due to its outstanding electrical and mechanical properties, namely, ultra-high Young's modulus and mechanical strength[2], superior electron mobility[3] and super low mass density. The application of graphene has provided a path to a new class of resonators and sensors in the past 15 years, such as pressure sensors[4–7], electromechanical actuator[8], resonators[9–16], microphones[17–20], nanodrums[21,22] and bio-sensor[23].

The unique mechanical and electrical properties of graphene also show that it is an interesting material for ultrasonic sensing. The large Young's modulus of graphene suggests graphene-based membranes can be easily designed to reach the high resonant frequency, typically in the range of Mega Hertz[11–14,16,21,24,25]. The superior electrical properties of graphene allow the development of electrical read-out for the electromechanical ultrasonic devices. The ultrasonic detection has been used in medical imaging[26], non-contact sensing[27], non-destructive testing[28], ultrasonic range finding[29] and ultrasound Identification[30]. The desired ultrasonic frequency is from 20 kHz and up to GHz dependent on the applications. Furthermore, previous work in graphene-based ultrasonic sensor has been reported to be detected in vacuum[14]. Apart from ultrasonic sensing, another application of the resonators with resonant frequency less than 200 kHz is to achieve microphones with good signal-to-noise ratio (SNR) and sensitivity. The resonant frequency in our previous work of graphene/PMMA capacitive microphone [31] has been observed

Citation: Title. *Journal Not Specified* **2023**, *1*, 0. https://doi.org/

Received:
Revised:
Accepted:
Published:

within audio frequency, which decreases the sensitivity of the microphones. In commercial capacitive microphones, the resonant frequency of diaphragms has been designed to be beyond the audio frequency range. However, in atmosphere, the vibrational magnitude of the graphene-based ultrasonic sensors can be difficult to be detected due to the presence of air damping.

To date, there is limited study on graphene-based resonators reported to cover the ultrasonic frequency range between 20 kHz to 1 MHz. To achieve relatively lower ultrasonic frequency range (below 1MHz), the larger size of graphene-base membranes is required, which increases the complexity of graphene transfer and the difficulty to suspend graphene-based membrane over the substrate without collapse. To address these two problems, the ultrasonic transducer[20] has been reported to be developed by the transfer of 66-layer graphene membrane onto the supporting frame and afterwards manually assembled to the bottom electrode. The air gap formed by the manual assembly of the graphene membrane and substrate is a variable parameter, which might decrease the consistency of device operation. The key in fabricating the graphene-based ultrasonic sensor for lower ultrasonic frequency is to develop a one-step process to control the air gap in order to avoid the manual assembly process which can decrease inconsistency in the device fabrication and operation.

In this work, a fully clamped graphene/PMMA closed cavity resonator at the resonant frequency less than 200 kHz will be presented. To avoid the membrane being transferred on the supporting ring and assembled onto the substrate afterwards, a one-step graphene dry transfer process, has been developed by our group[15]. The 6-layer graphene reinforced by 450 nm thick PMMA has been transferred directly onto the substrate and suspended fully over a closed circular cavity with a diameter of 0.5 mm and formed an air gap of 105 μm. The thin PMMA layer functions not only as the attachment between the graphene and the anchor of the substrate but also the supporting layer for the graphene to be suspended over the closed cavity. The air gap of 105 μm has been designed to minimize the effect of air damping. The sensor has been actuated mechanically, electro-statically and electro-thermally in atmosphere. It is the first time that the dynamic resonant characteristics of the graphene/PMMA ultrasonic closed cavity resonator have been determined.

2. Materials and Methods

The optical image of the graphene/PMMA ultrasonic closed cavity resonator is shown in Fig. 1.a. The graphene/PMMA membrane has been transferred onto the silicon dioxide on silicon substrate with the closed cavity, of which an air gap has been designed to be 105 μm. The squares at the corners of the chip have been patterned and etched into silicon to serve as electrodes. As the cross-section schematic of the device shown in Fig. 1.b, an air gap of 105 μm has been formed by the suspended membrane and the silicon substrate, which has been measured by Leica 150x optical microscope. The capacitance between the membrane and the substate has been calculated to be 16.5 fF. The graphene/PMMA membrane and the silicon substrate work as two plates for the capacitive structure. The natural frequency formula for the graphene/PMMA membrane can be determined by,

$$t_{\mathrm{eff}} = t_{\mathrm{g}} + t_{\mathrm{p}}, \tag{1}$$

$$\rho_{\mathrm{eff}} = \frac{\rho_{\mathrm{g}} t_{\mathrm{g}} + \rho_{\mathrm{p}} t_{\mathrm{p}}}{t_{\mathrm{g}} + t_{\mathrm{p}}}, \tag{2}$$

$$A_{\mathrm{m}} = \frac{\rho_{\mathrm{air}} R}{3 \rho_{\mathrm{eff}} t_{\mathrm{eff}}}, \tag{3}$$

$$f_{\mathrm{mn}} = \frac{\beta_{\mathrm{mn}}}{2\pi R} \sqrt{\frac{N_{\mathrm{i}} + N_{\mathrm{a}}}{\rho_{\mathrm{eff}} t_{\mathrm{eff}} (1 + A_{\mathrm{m}})}}, \tag{4}$$

where t and ρ are thickness and mass density of the material, t_{eff} and ρ_{eff} refer to the effective thickness and effective mass density for graphene (g)/PMMA (p) bi-layer membrane, R is the radius of the membrane, ρ_{air} refers to the air density, A_{m} is the air mass, N_{i} and

N_a represent the membrane's built-in tension and actuation tension which is caused by dynamic actuation, and β_{mn} is a dimensionless coefficient of the resonant mode.

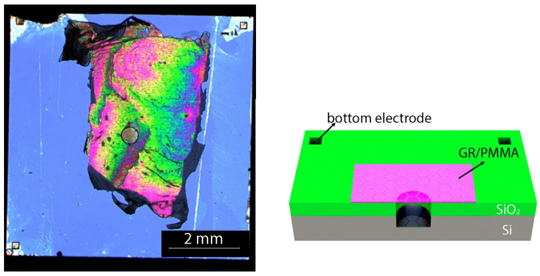

(a) **(b)**

Figure 1. The optical image (a) and cross-section schematic (b) of the closed cavity resonator with 105 µm gap.

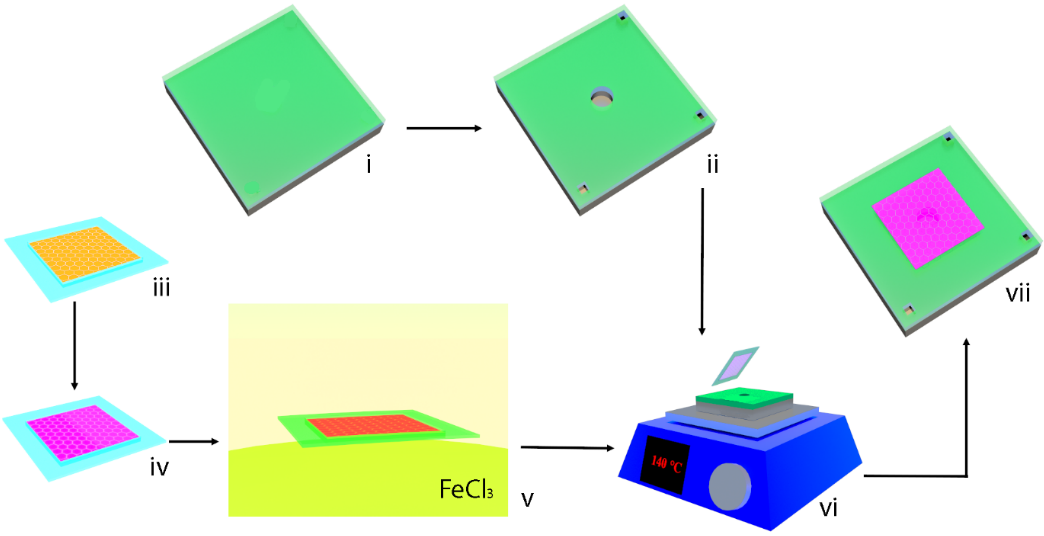

Figure 2. The fabrication schematic of the graphene/PMMA closed cavity ultrasonic sensor.

The fabrication process of the graphene/PMMA closed cavity ultrasonic sensor has been shown in Fig. 2. The preparation of the device's substrate has been shown in Fig. 2.i & ii, the 500 nm silicon dioxide has been deposited onto the silicon substrate. The circular cavity with the diameter of 500 μm, together with three square holes with 100 μm width that serve as electrodes have been patterned and etched into the silicon dioxide and silicon. The preparation of the graphene/PMMA membrane: (iii) the Kapton tape frame attached on the copper CVD graphene; (iv) PMMA spin-coated on the CVD graphene; (v) the copper foil etched by ferric chloride; The dry transfer of the graphene/PMMA membrane: (vi) graphene/PMMA membrane dry transferred on the substrate and the Kapton tape frame peeled off from membrane at the temperature of 140°C; (vii) the device cooled down in the air. Additionally, the dry graphene dry transfer method have also been reported in our previous publication [15]. In this work, the success rate of the fabrication process has been 100 % over two devices.

3. Results and discussion

3.1. Dynamic actuation

The graphene/PMMA ultrasonic resonator has been actuated mechanically, electro-statically and electro-thermally to characterize its dynamic behavior. For the mechanical actuation, the graphene/PMMA ultrasonic resonator has been placed and attached on the piezoelectric disk. By applying voltage to the piezoelectric disk, the ultrasound vibration has been generated and actuating the substrate of the resonator. For the electro-static actuation, silver paste has been attached on the graphene layer to work as the top electrodes. The patterns etched into the silicon with the resistivity of 1-10 Ωcm has been used as the bottom electrodes. The electro-static stress between the graphene membrane and the substrate has been generated by the voltage applied to the top and bottom electrodes. For the electro-thermal actuation, the thermal expansion of the membrane has been actuated by the voltage applied to the silver paste on the graphene layer. The dynamic characteristics have been measured by Polytec Laser Doppler Vibrometer (LDV). In addition to actuating the resonator by the signal with the frequency sweep, the sine-function signal of the membrane's resonant frequency has also been applied in order to provide the larger response time for the membrane to be actuated and to improve the accuracy of the dis-placement of the membrane which has been measured. All the measurements have been conducted on one device at room temperature and in atmosphere.

3.1.1. Mechanical actuation

For mechanical actuation, the varying AC voltage from 0.2 V to 3 V and constant 1 V DC voltage with the frequency sweep from 150 kHz to 220 kHz has been applied to the piezo-disk. The frequency response of the membrane has been shown in Fig. 3.a. The resonant frequency of the membrane has been measured to be around 163.15 kHz $\pm$0.2 % with a side band of around 169.487 kHz. The side band can be explained by the coupling between the membrane and substrate. The frequency peak at around 169 kHz has been observed with the graphene/PMMA membrane stuck on the silicon dioxide substrate anchor under mechanical actuation (Figure S1, Supporting Information). The frequency response measured under the frequency sweep at 0.1 V AC and 0.2 V AC seems to be similar, which can be explained by the response time at an ultrasonic frequency of around 163 kHz being too small for the membrane actuated at the lower AC voltages to respond and reach its maximum value. The quality factor at the resonant frequency has been estimated to be 49.45 $\pm$6.8 %.

3.1.2. Electro-static actuation

For electro-static actuation, the voltage of constant 1 V DC and varying AC voltage from 4 V and 9 V with frequency sweep between 120 kHz to 200 kHz have been applied be-tween the membrane and substrate. The frequency response of the graphene/PMMA membrane has been shown in Fig. 3.b. The resonant frequency has been measured to be 158.337 kHz $\pm$0.4 % with the side band observed at 169.265 kHz. The likely explanation of the side band is the coupling between the membrane and substrate. Like the mechanical actuation, the actuation stress (electro-static stress) has been vertical to the membrane. In addition, the side band frequency at the electro-static actuation has been observed to be similar to the side band frequency observed from the mechanical actuation (Fig. 3.a). The quality factor has been observed to be 25.64 $\pm$5.8 % at the resonant frequency.

3.1.3. Electro-thermal actuation

For electro-thermal actuation, the frequency response of the resonator actuated by in-creasing 1 V to 9 V AC and 1 V DC voltage applied to the silver paste on the graphene/PMMA membrane with the frequency range from 140 kHz to 220 kHz, has been illustrated in Fig. 3.c. The resonant frequency has been observed to be around 158.965 kHz $\pm$1.9 % and with the side band of around 187.851 kHz. The side band can be explained by the transition between the (1,1) mode and (0,2) mode (Figure S2, Sup-porting information). Under the electro-thermal actuation, the membrane has been heated when the AC voltage has been applied and the transition between the (1,1) mode and (0,2) mode can result from thermal stress in the membrane. Such a transition has not been observed in mechanical and electro-static actuation. Unlike the other two actuation methods where the actuation stress has been out-of-plane, in the case of electro-thermal actuation, the thermal expansion generated by the Joule heating has been in-plane. The likely explanation is that the in-plane actuation stress through the membrane has not generated the coupling between the membrane and substrate. In the cases of the other two actuation methods, the coupling between the membrane and substrate dominates vibration at the side band frequency and the transition with smaller amplitude has not been observed. At the resonant frequency, the quality factor has been detected to be 34.42 ±15.8 %.

3.2. Sensitivity of vibration amplitude

The vibration amplitude of graphene/PMMA membrane over the closed cavity has been shown in Fig. 4. The membrane has been actuated by sinusoidal signal at the resonant frequencies corresponding to different actuation methods. The amplitude of the membrane has been observed to be linear with the increasing AC voltage under the mechanical and electro-static actuation, as illustrated in Fig. 4.a and Fig. 4.b. In the case of the electro-thermal actuation, the graphene/PMMA membrane has been actuated by the thermal stress which has been generated by Joule heating. The thermal stress is linear with the Joule heating and thus is quadratic with the input AC voltage. As shown in Fig. 4.c, the quadratic relation between the amplitude and input AC voltage from 1 V to 8 V has been observed. At a voltage of 9 V AC, the amplitude which has not been shown to fit with the parabola function can be explained by the membrane's resonant frequency being shifted by the increasing AC voltage. At 9 V AC, the resonant frequency of the mem-brane over the closed cavity has been measured to be 161.914 kHz, with the frequency shift of around 5 kHz away from the actuated sinusoidal signal at frequency of 156.914 kHz (Fig. 4). The amplitude at the frequency with around 5 kHz shifted from the resonant frequency has been smaller than the amplitude measured at the resonant frequency.

The dynamic behavior of graphene/PMMA closed cavity ultrasonic sensor is summarized in Table 1. Under electro-static actuation, the explanation of the small amplitude meausred in the frequency sweep is the air gap of around 105 μm, which forms a small capacitance between the membrane and substrate. The measured resonant frequency has been observed to change with the actuation methods. In the cases of electro-static and electro-thermal actuation, the measured resonant frequency is smaller compared to the mechanical frequency, which can be explained by capacitive softening[32–34] and electro-thermal softening[35].

3.3. Frequency shift and quality factor

In mechanical and electro-static actuation, change in frequency shift and quality factor versus the input signal has been detected to be relatively small compared to the electro-thermal case as shown in Fig. 5.a to c.

In the case of the electro-thermal actuation, the change in quality factor can be temperature-related. The frequency shift at resonance is evident in the frequency response (Fig. 3.c). The relationship between the frequency shift and the AC voltage has been plotted in Fig. 5.c. The resonant frequency at 9 V AC has been upshifted to be 3.8 % from the frequency

Table 1. The dynamic characteristics of graphene/PMMA closed cavity ultra-sonic sensor.

Actuation methods	Measured resonant frequency	Quality factor	Actuated sinusoidal signal frequency	Varying input signal range of sinusoidal signal	Sensitivity of vibration amplitude actuated by sinusoidal signal
Mechanical	163.150 kHz ±0.2%	49.45 ±6.8%	163.156 kHz	0.1 V to 2 V AC	14 nm/V
Electro-static	158.337 kHz ±0.4%	25.64 ±5.8%	158.640 kHz	1 V to 9 V AV	0.01 nm/V
Electro-thermal	158.965 kHz ±1.9%	34.42 ±15.8%	156.914 kHz	1 V to 9 V AV	0.002 nm/V^2

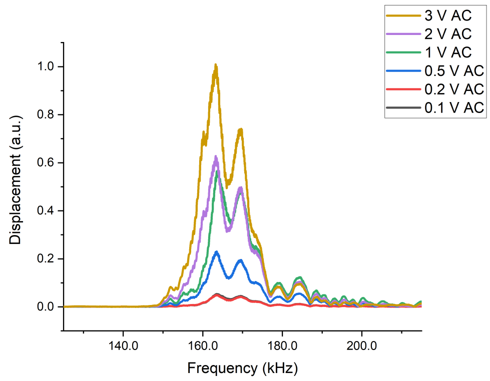

(a)

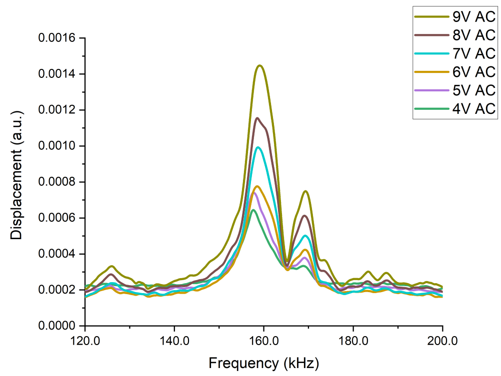

(b)

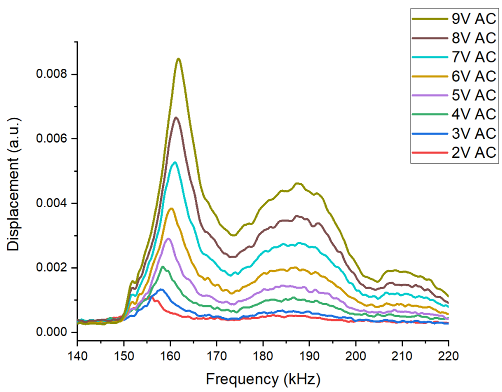

(c)

Figure 3. The frequency response of the membrane under: (a) mechanical actuation with the input voltage from 0.1 V to 3 V AC and 1 V DC as well as by the frequency sweep from 150 kHz to 220 kHz; (b) electro-static actuation with the voltage of constant 1 V DC voltage and varying AC from 4 V to 9V with the frequency sweep between 120 kHz and 200 kHz; (c) electro-thermal frequency sweep signal with 2-9 V AC and 1 V DC be-tween 140 kHz and 220 kHz.

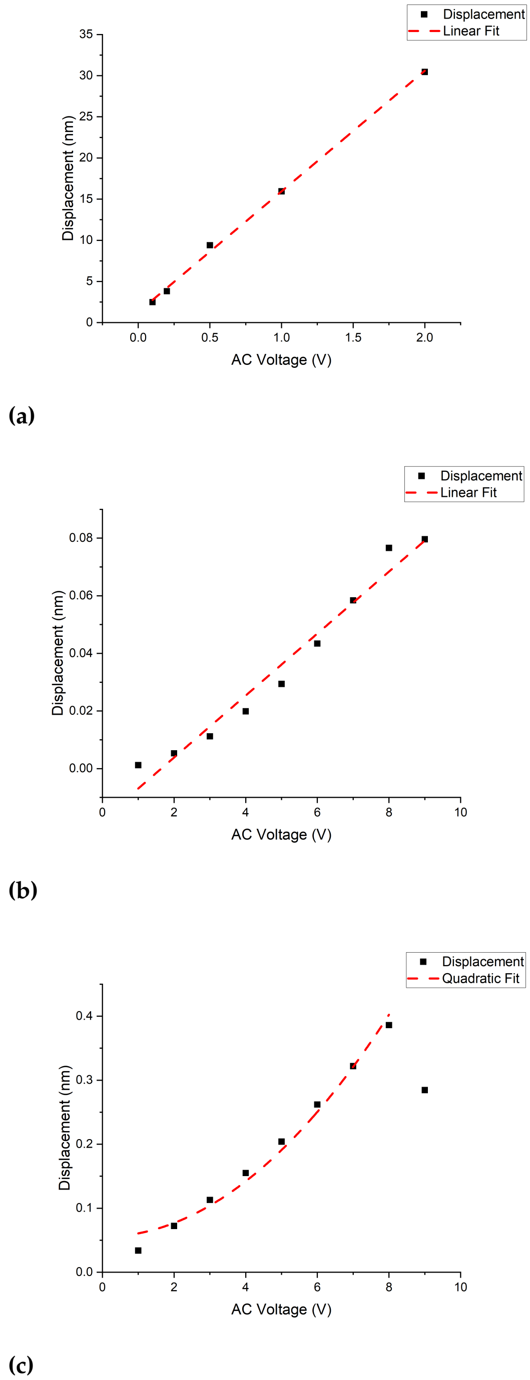

Figure 4. The amplitude of the membrane under: (a) mechanical actuation (0.1 V AC to 2 V AC and constant 1 V DC) at 163.156 kHz with linear fitting; (b) electro-static actuation at 158.640 kHz with signal of the AC voltage changing from 1 V to 9 V and constant 1 V DC, with linear fitting; (c) under electro-thermal actuation at 156.914 kHz with the voltage of 1-9 V AC and 1 V DC along with parabola fitting.

at 2 V AC. The upshift of the resonant frequency as the AC voltage increase can be a result of the negative thermal expansion coefficient of graphene[36]. Graphene shrinks as its temperature rises and therefore, the resonant frequency increases with rising AC voltage[16]. The fitting (red dash) of the frequency shift corresponds to $V_{ac}^{\frac{2}{3}}$ .The nonlinearity of the frequency shift can be explained by the air damping inside the perfectly sealed closed cavity.

As shown in Table 1, the quality factor when the membrane is actuated mechanically has been observed to be the maximum among the three actuation methods. The piezo-electric disk has been directly in contact with the substrate during mechanical actuation and therefore the input ultrasonic energy has been the largest among the three actuation methods. The quality factor measured under electro-static actuation has been measured to be the minimum among the three actuation methods, which is related to the smallest dis-placement observed compared to the other two actuation methods. The air gap of 105 μm results in a capacitance of 16.5 fF and the signal generated by the electro-static stress between the membrane and substrate is relatively small compared to the other two actuation methods.

The change in the quality factor has been studied in the resonator under the electro-thermal actuation. The quality factor has been measured to increase from around 36 to 40 when the AC voltage rises from 2 V and 3 V. The decrease of the quality factor has been observed when the AC voltage changes from 3 V to 8 V. A small increase of the quality factor has been measured when the AC voltage increased from 8 V to 9 V, as shown in Fig. 5.c. Unlike the mechanical and electro-static actuation, frequency upshift has been observed in the resonator under electro-thermal actuation. The decrease in the quality fac-tor suggests that the energy dissipated in the resonator is larger than the energy stored at resonant frequency[37], which can be explained by the higher damping[16] or more surface loss[38] of the energy as higher AC voltage is applied to the membrane. The boost of thermal gradient in the membrane with increasing AC voltage might enhance the thermoelastic damping, which increases the dissipation[37]. Additionally, the possible surface stress increase with rising temperature might enlarge the surface loss, which results in energy dissipation[38,39].

3.4. Mode shape

The mode shapes at the resonant frequencies by different actuation methods have been shown in Fig. 6. The observation of (1,1) at the resonant frequencies by the three actu-ations methods has been caused by the closed cavity design and the impermeability of graphene[40]. The air leakage has been extremely small as the graphene/PMMA membrane has been sealed the closed cavity perfectly. Thus, the (0,1) mode which requires the large change of the air volume inside the cavity has been prevented and not been observed. Fig. 6 (a) to (c) are placed at the same x-y plane to compare the orientations under different actuation schemes. The orientation of (1,1) mode shape has been observed to be similar in the mechanical and electrostatic actuation, which can be explained by the direction of the mechanical stress and electro-static stress has been vertical. In the case of electro-thermal actuation, the orientation of the (1,1) mode shape has been related to the position of the membrane electrodes.

3.5. Strain analysis

The overall tension and strain can be derived from equation (4) and results are shown in Table 2. In the case of the mechanical actuation, the tension has been estimated to be the largest among the different actuation methods.

4. Conclusions

It is the first time that graphene-based closed cavity ultrasonic resonator has been fab-ricated and actuated in atmosphere successfully. Using graphene dry transfer method

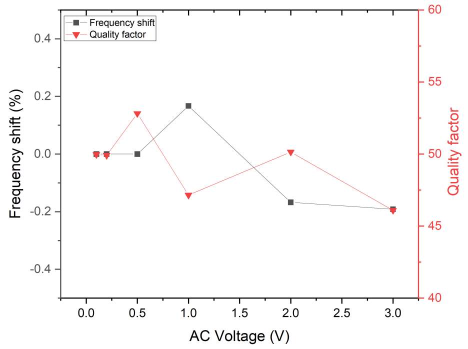

(a)

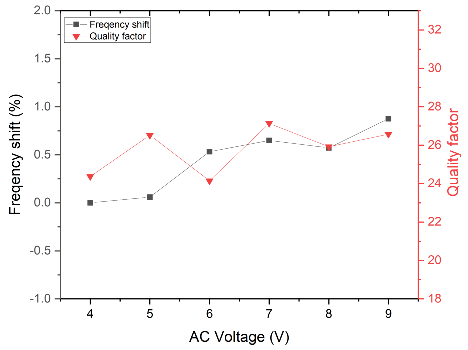

(b)

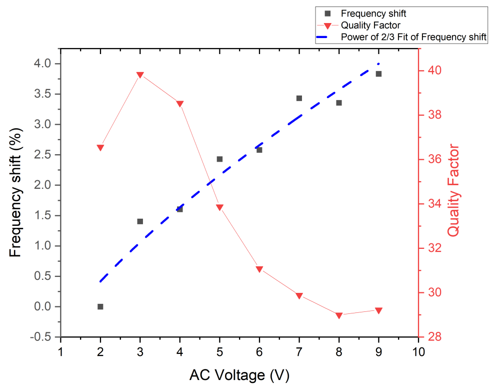

(c)

Figure 5. The frequency shift and quality factor of graphene/PMMA resonator under: (a) mechanical actuation (b) electro-static actuation; (c) electro-thermal actuation.

Table 2. Overall tension and strain in the graphene/PMMA membrane deducted from the measured resonant frequency.

Actuation methods	Frequency (kHz)	Tension (N/m)	Strain (%)
Mechanical	163.150	3.00	0.0813
Electro-static	158.384	2.83	0.0766
Electro-thermal	158.965	2.85	0.0772

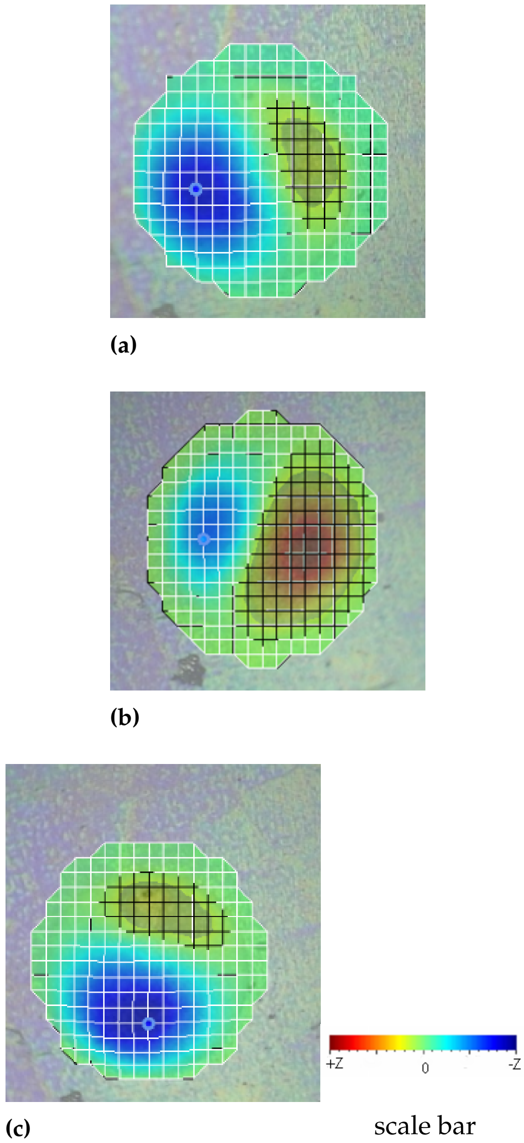

Figure 6. The mode shape of graphene/PMMA membrane over closed cavity resonator at resonant frequencies under: (a) mechanical actuation (0.5 V AC, 1 V DC) ((b) electro-static actuation (3V AC, 1 V DC); (c) electro-thermal actuation (3V AC, 1 V DC).

with Kapton tape as the supporting frame developed by our group, the graphene/PMMA closed cavity sensor at a resonant frequency of around 160 kHz has been fabricated. The graphene/PMMA closed cavity resonator has been actuated mechanically, electro-statically and electro-thermally. The amplitude of the membrane has been observed to be linear with AC voltage for the mechanical and electro-static actuation and quadratic with AC voltage for the electro-thermal actuation. The membrane has been observed to exhibit (1,1) mode at the resonant frequencies. The membrane can be tuned up to 4% by varying AC voltage via the electrodes connected to the graphene/PMMA membrane and nonlinear frequency shift under electro-thermal actuation has been detected. The strain in the membrane under the three actuation methods has been estimated to be around 0.08%. The device shows the possibility of applying graphene as ultrasonic detectors and opens a door to fabricating graphene-based ultrasonic sensors at the lower ultrasonic frequency of less than 200 kHz.

Supplementary Materials: The following supporting information can be downloaded at: The Frequency response of the substrate under mechanical actuation; Transition between (1,1) mode and (0,2) mode under electro-thermal actuation; Raman spectrum on graphene layer.

Acknowledgments: The authors acknowledge the financial support of the UK Engineering and Physical Sciences Research Council (EPSRC). The authors genuinely acknowledge the assistance from Dr. Andrey Gromov for Raman spectroscopy measurements.

References

1. Novoselov, K.S.; Geim, A.K.; Morozov, S.V.; Jiang, D.; Zhang, Y.; Dubonos, S.V.; Grigorieva, I.V.; Firsov, A.A. Electric field effect in atomically thin carbon films. *Science* **2004**, *306*, 666–9. https://doi.org/10.1126/science.1102896.
2. Lee, C.; Wei, X.; Kysar, J.W.; Hone, J. Measurement of the elastic properties and intrinsic strength of monolayer graphene. *Science* **2008**, *321*, 385–8. https://doi.org/10.1126/science.1157996.
3. Bolotin, K.I.; Sikes, K.J.; Jiang, Z.; Klima, M.; Fudenberg, G.; Hone, J.; Kim, P.; Stormer, H.L. Ultrahigh electron mobility in suspended graphene. *Solid State Communications* **2008**, *146*, 351–355. https://doi.org/10.1016/j.ssc.2008.02.024.
4. Aguilera-Servin, J.; Miao, T.; Bockrath, M. Nanoscale pressure sensors realized from suspended graphene membrane devices. *Applied Physics Letters* **2015**, *106*. https://doi.org/10.1063/1.4908176.
5. Berger, C.; Phillips, R.; Centeno, A.; Zurutuza, A.; Vijayaraghavan, A. Capacitive pressure sensing with suspended graphene-polymer heterostructure membranes. *Nanoscale* **2017**, *9*, 17439–17449. https://doi.org/10.1039/c7nr04621a.
6. Dolleman, R.J.; Davidovikj, D.; Cartamil-Bueno, S.J.; van der Zant, H.S.; Steeneken, P.G. Graphene Squeeze-Film Pressure Sensors. *Nano Lett* **2016**, *16*, 568–71. https://doi.org/10.1021/acs.nanolett.5b04251.
7. Wang, Q.; Hong, W.; Dong, L. Graphene "microdrums" on a freestanding perforated thin membrane for high sensitivity MEMS pressure sensors. *Nanoscale* **2016**, *8*, 7663–71. https://doi.org/10.1039/c5nr09274d.
8. Zhu, S.E.; Shabani, R.; Rho, J.; Kim, Y.; Hong, B.H.; Ahn, J.H.; Cho, H.J. Graphene-based bimorph microactuators. *Nano Lett* **2011**, *11*, 977–81. https://doi.org/10.1021/nl103618e.
9. Al-mashaal, A.K.; Wood, G.S.; Torin, A.; Mastropaolo, E.; Newton, M.J.; Cheung, R. Dynamic behavior of ultra large graphene-based membranes using electrothermal transduction. *Applied Physics Letters* **2017**, *111*. https://doi.org/10.1063/1.5007327.
10. Al-mashaal, A.K.; Wood, G.S.; Torin, A.; Mastropaolo, E.; Newton, M.J.; Cheung, R. Tunable Graphene-Polymer Resonators for Audio Frequency Sensing Applications. *IEEE Sensors Journal* **2019**, *19*, 465–473. https://doi.org/10.1109/jsen.2018.2877463.
11. Bunch, J.S.; van der Zande, A.M.; Verbridge, S.S.; Frank, I.W.; Tanenbaum, D.M.; Parpia, J.M.; Craighead, H.G.; McEuen, P.L. Electromechanical resonators from graphene sheets. *Science* **2007**, *315*, 490–3. https://doi.org/10.1126/science.1136836.
12. Chen, T.; Mastropaolo, E.; Bunting, A.; Cheung, R. Observation of second flexural mode enhancement in graphene resonators. *Electronics Letters* **2015**, *51*, 1014–1016. https://doi.org/10.1049/el.2015.0361.
13. Lee, S.; Chen, C.; Deshpande, V.V.; Lee, G.H.; Lee, I.; Lekas, M.; Gondarenko, A.; Yu, Y.J.; Shepard, K.; Kim, P.; et al. Electrically integrated SU-8 clamped graphene drum resonators for strain engineering. *Applied Physics Letters* **2013**, *102*. https://doi.org/10.1063/1.4793302.
14. Verbiest, G.J.; Kirchhof, J.N.; Sonntag, J.; Goldsche, M.; Khodkov, T.; Stampfer, C. Detecting Ultrasound Vibrations with Graphene Resonators. *Nano Lett* **2018**, *18*, 5132–5137. https://doi.org/10.1021/acs.nanolett.8b02036.
15. Xu, J.; Wood, G.S.; Al-mashaal, A.K.; Mastropaolo, E.; Newton, M.J.; Cheung, R. Realization of Closed Cavity Resonator Formed by Graphene-PMMA Membrane for Sensing Audio Frequency. *IEEE Sensors Journal* **2020**, *20*, 4618–4627. https://doi.org/10.1109/jsen.2020.2966415.
16. Ye, F.; Lee, J.; Feng, P.X. Electrothermally Tunable Graphene Resonators Operating at Very High Temperature up to 1200 K. *Nano Lett* **2018**, *18*, 1678–1685. https://doi.org/10.1021/acs.nanolett.7b04685.

17. Todorović, D.; Matković, A.; Milićević, M.; Jovanović, D.; Gajić, R.; Salom, I.; Spasenović, M. Multilayer graphene condenser microphone. *2D Materials* **2015**, *2*. https://doi.org/10.1088/2053-1583/2/4/045013.
18. Woo, S.; Han, J.H.; Lee, J.H.; Cho, S.; Seong, K.W.; Choi, M.; Cho, J.H. Realization of a High Sensitivity Microphone for a Hearing Aid Using a Graphene-PMMA Laminated Diaphragm. *ACS Appl Mater Interfaces* **2017**, *9*, 1237–1246. https://doi.org/10.1021/acsami.6b12184.
19. Wood, G.S.; Torin, A.; Al-mashaal, A.K.; Smith, L.S.; Mastropaolo, E.; Newton, M.J.; Cheung, R. Design and Characterization of a Micro-Fabricated Graphene-Based MEMS Microphone. *IEEE Sensors Journal* **2019**, *19*, 7234–7242. https://doi.org/10.1109/jsen.2019.2914401.
20. Zhou, Q.; Zheng, J.; Onishi, S.; Crommie, M.F.; Zettl, A.K. Graphene electrostatic microphone and ultrasonic radio. *Proc Natl Acad Sci U S A* **2015**, *112*, 8942–6. https://doi.org/10.1073/pnas.1505800112.
21. Davidovikj, D.; Poot, M.; Cartamil-Bueno, S.J.; Van Der Zant, H.S.J.; Steeneken, P.G. On-chip Heaters for Tension Tuning of Graphene Nanodrums. *Nano Letters* **2018**, *18*, 2852–2858. https://doi.org/10.1021/acs.nanolett.7b05358.
22. Wong, C.L.; Annamalai, M.; Wang, Z.Q.; Palaniapan, M. Characterization of nanomechanical graphene drum structures. *Journal of Micromechanics and Microengineering* **2010**, *20*. https://doi.org/10.1088/0960-1317/20/11/115029.
23. Pumera, M. Graphene in biosensing. *Materials Today* **2011**, *14*, 308–315. https://doi.org/10.1016/s1369-7021(11)70160-2.
24. Garcia-Sanchez, D.; van der Zande, A.M.; Paulo, A.S.; Lassagne, B.; McEuen, P.L.; Bachtold, A. Imaging mechanical vibrations in suspended graphene sheets. *Nano Lett* **2008**, *8*, 1399–403. https://doi.org/10.1021/nl080201h.
25. Singh, R.; Nicholl, R.J.T.; Bolotin, K.I.; Ghosh, S. Motion Transduction with Thermo-mechanically Squeezed Graphene Resonator Modes. *Nano Lett* **2018**, *18*, 6719–6724. https://doi.org/10.1021/acs.nanolett.8b02293.
26. Ophir, J.; Maklad, N.F. Digital scan converters in diagnostic ultrasound imaging. *Proceedings of the IEEE* **1979**, *67*, 654–664. https://doi.org/10.1109/proc.1979.11289.
27. Green, R. E., J. Non-contact ultrasonic techniques. *Ultrasonics* **2004**, *42*, 9–16. https://doi.org/10.1016/j.ultras.2004.01.101.
28. Drinkwater, B.W.; Wilcox, P.D. Ultrasonic arrays for non-destructive evaluation: A review. *NDT & E International* **2006**, *39*, 525–541. https://doi.org/10.1016/j.ndteint.2006.03.006.
29. Hong, H.; Yongtian, W.; Dayuan, Y. A low-cost dynamic range-finding device based on amplitude-modulated continuous ultrasonic wave. *IEEE Transactions on Instrumentation and Measurement* **2002**, *51*, 362–367. https://doi.org/10.1109/19.997838.
30. Alexandrov, A.V. Ultrasound identification and lysis of clots. *Stroke* **2004**, *35*, 2722–5. https://doi.org/10.1161/01.STR.0000143321.37482.b3.
31. Xu, J.; Wood, G.S.; Mastropaolo, E.; Newton, M.J.; Cheung, R. Realization of a graphene/PMMA acoustic capacitive sensor released by silicon dioxide sacrificial layer. *ACS Applied Materials & Interfaces* **2021**, *13*, 38792–38798.
32. Fung, W.Y.; Dattoli, E.N.; Lu, W. Radio frequency nanowire resonators and in situ frequency tuning. *Applied Physics Letters* **2009**, *94*. https://doi.org/10.1063/1.3139750.
33. Kozinsky, I.; Postma, H.W.C.; Bargatin, I.; Roukes, M.L. Tuning nonlinearity, dynamic range, and frequency of nanomechanical resonators. *Applied Physics Letters* **2006**, *88*. https://doi.org/10.1063/1.2209211.
34. Wu, C.C.; Zhong, Z. Capacitive spring softening in single-walled carbon nanotube nanoelectromechanical resonators. *Nano Lett* **2011**, *11*, 1448–51. https://doi.org/10.1021/nl1039549.
35. Chen, K.; Schweizer, K.S. Theory of Yielding, Strain Softening, and Steady Plastic Flow in Polymer Glasses under Constant Strain Rate Deformation. *Macromolecules* **2011**, *44*, 3988–4000. https://doi.org/10.1021/ma200436w.
36. Lau, C.N.; Bao, W.; Velasco, J. Properties of suspended graphene membranes. *Materials Today* **2012**, *15*, 238–245. https://doi.org/10.1016/s1369-7021(12)70114-1.
37. Schmid, S.; Villanueva, L.G.; Roukes, M.L., Quality Factor. In *Fundamentals of Nanomechanical Resonators*; 2016; book section Chapter 2, pp. 57–90. https://doi.org/10.1007/978-3-319-28691-4_2.
38. Lee, J.; Wang, Z.; He, K.; Shan, J.; Feng, P.X.L. High Frequency MoS2 Nanomechanical Resonators. *ACS Nano* **2013**, *7*, 6086–6091, [https://doi.org/10.1021/nn4018872]. PMID: 23738924, https://doi.org/10.1021/nn4018872.
39. Jinling, Y.; Ono, T.; Esashi, M. Energy dissipation in submicrometer thick single-crystal silicon cantilevers. *Journal of Microelectromechanical Systems* **2002**, *11*, 775–783. https://doi.org/10.1109/jmems.2002.805208.
40. Bunch, J.S.; Verbridge, S.S.; Alden, J.S.; van der Zande, A.M.; Parpia, J.M.; Craighead, H.G.; McEuen, P.L. Impermeable atomic membranes from graphene sheets. *Nano Lett* **2008**, *8*, 2458–62. https://doi.org/10.1021/nl801457b.